

RINOPOLYCRETE - TOWARDS A CEMENT-FREE AND FULLY RECYCLED CONCRETE



FCT PROJECT

PTDC/ECI-COM/29196/2017

**Recycled inorganic polymer concrete - Towards a cement-free and fully recycled concrete
(RInoPolyCrete)**

Task 2 - Report 2

Further optimization of the alkaline solution for the production of mortars with alkali activated municipal solid waste incinerator bottom ashes

July, 2019

Funding FCT/POCI



Governo da República Portuguesa



União Europeia FEDER

FCT Fundação para a Ciência e a Tecnologia
MINISTÉRIO DA CIÊNCIA E DO ENSINO SUPERIOR Portugal

TABLE OF CONTENTS

1	INTRODUCTION	1
2	MATERIALS AND METHODS.....	2
2.1	WASTE PRECURSORS FOR ALKALI ACTIVATION.....	2
2.1.1	<i>Water treatment sludge.....</i>	2
2.1.2	<i>Water treatment sludge ash.....</i>	2
2.1.3	<i>Municipal solid waste incinerator bottom ash.....</i>	2
2.1.4	<i>Electric arc furnace slag.....</i>	2
2.2	ALKALINE ACTIVATOR	2
2.3	FINE AGGREGATES	3
2.4	CHARACTERIZATION TESTS.....	3
2.5	MIXING METHODOLOGIES	4
3	RESULTS AND DISCUSSION	5
3.1	CHARACTERIZATION OF THE WASTE PRECURSORS	5
3.1.1	<i>Scanning electron microscopy/Energy dispersive X-ray spectroscopy.....</i>	5
3.1.2	<i>X-ray diffraction.....</i>	10
3.1.3	<i>XRF.....</i>	Error! Bookmark not defined.
3.1.4	<i>pH.....</i>	13
3.1.5	<i>Quantification of metallic aluminium in MIBA.....</i>	14
3.1.6	<i>Pozzolanic activity index</i>	18
3.2	FRESH STATE PROPERTIES	18
3.2.1	<i>Density</i>	18
3.2.3	<i>Workability.....</i>	20
3.3	HARDENED STATE PERFORMANCE	21
3.3.1	<i>Compressive strength.....</i>	21
3.3.2	<i>Flexural strength.....</i>	25
4	CONCLUSIONS	26
	REFERENCES	27

FIGURE CAPTIONS

Figure 1 - Particle size distribution of the fine aggregates	3
Figure 2 - SEM micrographs of EAFS	6
Figure 3 - EDS coupled to SEM of EAFS	7
Figure 4 - SEM micrographs of untreated SWTP	7
Figure 5 - EDS coupled to SEM of untreated SWTP	8
Figure 6 - SEM micrographs of ASWTP: (a) 500 amplification; (b) 1,000 amplification.....	9
Figure 7 - EDS coupled to SEM for ASWTP treated at 700 °C	9
Figure 8 - SEM micrographs of MIBA	10
Figure 9 - EDS coupled to SEM of MIBA	10
Figure 10 - XRD pattern of SWTP (a) and ASWTP (b).....	12
Figure 11 - XRD pattern of MIBA	12
Figure 12 - XRD pattern for EAFS.....	12
Figure 13 - Hydrogen production over time of MIBA samples.....	16
Figure 14 - Density in the fresh state	19
Figure 15 - Density in the fresh state of M1, M2 and M3	20
Figure 16 - Workability of the mortars	21
Figure 17 - Compressive strength of all mortars	22
Figure 18 - Compressive strength of the control mixes	22
Figure 19 - Compressive strength of the mortars for methodology 1	24
Figure 20 - Compressive strength of the mortars for methodology 2.....	24
Figure 21 - Compressive strength of the mortars for methodology 3.....	24
Figure 22 - Flexural strength of the control mortars.....	25
Figure 23 - Flexural strength of the mortars for methodology 1	25

Figure 24 - Flexural strength of the mortars for methodology 2.26

Figure 25 - Flexural strength of the mortars for methodology 326

TABLE CAPTIONS

Table 1 - Composition of the mortars	5
Table 2 - Chemical composition of MIBA (% by mass)	13
Table 3 - Measurements made in triplicate for 0.1 g of pure metallic aluminium	15
Table 4 - Measurements made in triplicate for 10 g of MIBA	16

ACRONYMS

MIBA	Municipal solid waste incinerator bottom ash
EAFS	Electric arc furnace slag
SWTP	Sludge from a water treatment plant
ASWTP	Ash sludge from a water treatment plant
AAM	Alkali-activated materials
NaOH	Sodium hydroxide
SEM	Scanning electron microscopy
XRD	X-ray diffraction
XRF	X-ray fluorescence
EDS	Energy dispersive X-Ray spectroscopy
pH	Hydrogen potential
P	Polycarboxylate
L	Lignosulfonate
N	Naphthalene
M	Melamine

1 INTRODUCTION

The knowledge and analysis of the physicochemical and microstructural properties of precursors used in the manufacture of alkali-activated materials corresponds to the basis of an adequate formulation of these materials according to a scientific method, since it allows a more precise combination at all subsequent stages [1-4], since the composition of the precursor and in particular the vitreous or amorphous phase, as well as the presence of minor components, will largely determine the type of activator to be used, its concentration and the components of the reaction products [5]. The most relevant characterization tests correspond to: scanning electron microscopy (SEM), which reveals the morphology of the elements, as well as the elemental components described semi-quantitatively by energy dispersive X-ray spectroscopy (EDS) coupled to SEM; X-ray diffraction (XRD) and X-ray fluorescence (XRF), which exposes the crystalline phases present in the material and that displays the compositional content in terms of the oxides present, respectively, and allows the quantification of the amorphous phases for each of the oxides present [6-8]; the pH, which is an important chemical variable since alkali activation occurs at a high pH level; and the absorption of water, directly related to the amount of water necessary to achieve adequate workability.

Another important characteristic is the pozzolanic activity, since the literature demonstrates that, if the precursor material is capable of replacing cement as a supplementary cementing material in construction materials [9], it can also be chemically activated with the use of an alkaline activator. Likewise, it is important to perform specific tests on precursors when they have special characteristics. This is the case of municipal solid waste incinerator bottom ash (MIBA) as it can contain a notable amount of metallic aluminum, which reacts upon contact with water in an alkaline medium, generating hydrogen gas. This leads to the formation of bubbles in the materials' plastic state and subsequent porosity in the hardened state [10-12].

Tyrer [13] mentions in his work two alternatives for the removal or pretreatment of aluminum in MIBA, in order to eliminate or minimize the expansion caused by hydrogen, the first corresponds to the direct oxidation of the metal at high temperatures by citing the work of Qiao et al. [14] and the second the alkaline pretreatments, referring Rübner et al. [15].

The present report is divided in two sections. The first one corresponds to the characterization of four different precursors: electric arc furnace slag (EAFS), sludge from a water treatment plant (SWTP), ash sludge from a water treatment plant (ASWTP) and MIBA. For the latter, a second stage was developed, in which six different methodologies of mortar preparation were developed in order to evaluate the best way under which it is possible to obtain the best results of compressive strength, by controlling the release of hydrogen in the plastic state.

2 MATERIALS AND METHODS

2.1 Waste precursors for alkali activation

2.1.1 Water treatment sludge

Pre-dried sludge from the potable water treatment plant in Lisbon (Empresa Portuguesa das Águas Livres - EPAL SA) was collected from the output of the sedimentation stage.

2.1.2 Water treatment sludge ash

Sludge from EPAL, described in the previous section, was incinerated at about 700 °C.

2.1.3 Municipal solid waste incinerator bottom ash

Bottom ash was gathered from the incineration of solid waste from the Valorsul treatment plant, located in São João da Talha, in the municipality of Loures, Portugal.

2.1.4 Electric arc furnace slag

Electric arc furnace slag, is one of the by-products of the steel smelting in the Siderurgia Nacional de Portugal, provided by HARSCO

2.2 Alkaline activator

Sodium hydroxide (NaOH) in the solid state, with 99% purity, was used to prepare a 2.5 M solution. A low concentration was selected since the high calcium content present in MIBA and EAFS is insolubilized in high concentrations of sodium hydroxide [16, 17]. Drinking water

meeting the Portuguese requirements gal was used in the preparation of the alkali activator, as it is widely available.

2.3 Fine aggregates

Two siliceous sands were used complying with EN 12620 [18]; coarse sand with $D < 4$ mm, water absorption of 0.3% and dry volumetric mass of 2690 kg/m^3 ; and fine sand with $D < 1$ mm, water absorption of 0.2% and dry volumetric mass of 2690 kg/m^3 . Figure 1 presents the grain size distribution of the fine and coarse sands.

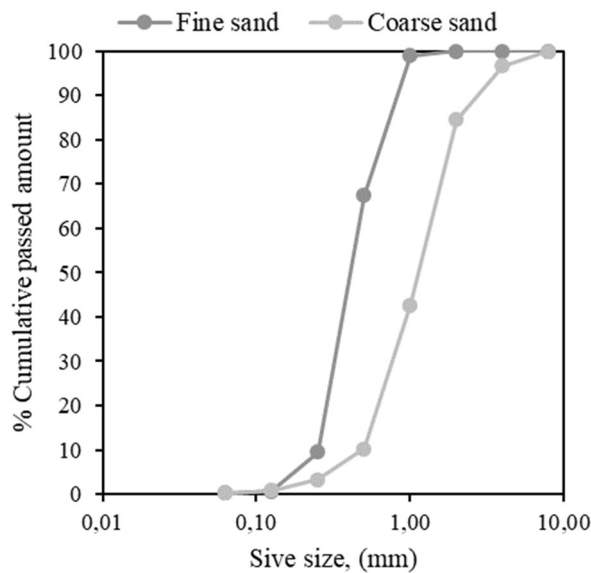


Figure 1 - Particle size distribution of the fine aggregates

2.4 Characterization tests

All samples were characterized with the following tests: electron microscopy coupled with EDS; X-ray diffraction (XRD) and pH. The aluminium quantification, X-ray fluorescence, (XRF) and pozzolanic activity with the modified Chappelle test were carried out exclusively in the MIBA sample.

2.5 Mixing methodologies

Two families of mortars with EAFS, with alkaline activator to slag ratios of 0.35 and 0.50, were produced. To determine the optimum mixing method of MIBA with the alkaline activator and the fine aggregates, mortars were prepared using six different methodologies, in order to select the most appropriate one in terms mitigating the production of hydrogen gas in the alka-lization reaction of metallic aluminium. Each methodology is described as follows:

- ✓ Methodology 1 (M1): The alkaline solution was prepared 24 hours before the prepara-tion of mortars. Aggregate was added 30 s after mixing MIBA with the alkaline solu-tion, then 15 min of mixing combining slow and fast agitation, finally 45 min resting.
- ✓ Methodology 2 (M2): The alkaline activator was prepared 24 hours before the prepara-tion of mortars. 15 min of mixing MIBA with the alkali solution in rapid agitation, then 45 min resting. Finally, the aggregates were added and mixed for 5 mins.
- ✓ Methodology 3 (M3): The aggregates were added 30 s after MIBA with a cold alkaline activator (4 °C) using slow mechanical stirring, then 15 min of fast mixing [19].
- ✓ Methodology 4 (M4): The alkaline activator together with MIBA were heated at 80 °C on a magnetic plate for 2 hours, then left for 2 more hours and finally mixed with the aggregates for 5 minutes [20].
- ✓ Methodology 5 (M5): The alkaline activator was prepared and MIBA was immediately added, then the mix was left to rest for 24 hours. After that, it was mixed with the aggregates for 5 minutes.
- ✓ Methodology 6 (M6): The alkaline activator was prepared with hot water at 50 °C. A temperature of 80 °C was reached when adding solid NaOH and immediately mixed with MIBA for one hour plus one hour of rest. Finally, the aggregates were added and mixed for 5 mins.

All mortar families were prepared and tested according to the EN-EP 196-2006 standard [21] For methodologies M1, M2 and M3, the following water reducing admixtures were used for the preparation of the mortars: polycarboxylate (P), lignosulfonate (L), naphthalene (N) and melamine (M). A control mortar without superplasticizer was also produced. Table 1 shows

mortars' composition within the abovementioned methodologies.

The following properties were evaluated for the processed mortars: fresh-state density and workability[22] and hardened state flexural strength and compressive strength[21].

Table 1 - Composition of the mortars

MIBA (g)	Fine aggregates (g)	NaOH (a)	Water (ml)	Superplasticizer (%)
450	1350	23	225	1

3 RESULTS AND DISCUSSION

3.1 Characterization of the waste precursors

3.1.1 Scanning electron microscopy/Energy dispersive X-ray spectroscopy

The morphological characterization of the samples was carried out in the SEM of IST's Department of Mechanical Engineering, which corresponds to a brand microscope HITACHI model S-2400. The samples were coated with Au-Pd alloy prior to observation to avoid electrical charge accumulation. In relation to the elemental composition, the SEM equipment was coupled to a detector of Energy Dispersive X-Ray Spectroscopy (EDS) brand BRUEKER EDS. This equipment determines, semi-quantitatively, atomic quantities of the different elements present in the sample, which is relevant to confirm the elements present in the mineralogical phases reported by the XRD analysis.

Figure 2a shows scattered and angular morphology of EAFS particles, typical of oxides when they break. Irregular, porous and isolated particles are observed, which is consistent with the findings of other authors, such as Santamaria et al. [23], who characterized EAFS microstructure for various applications in Civil Engineering. Similarly, the presence of smaller particles on the surface of larger particles, which have a lower density, is notable (Figure 2b). They mentioned in their work that low density particles are generated by the high temperatures at which this waste is generated, which results in the release of gases causing high porosity. This also agrees with the results of Alinezhad et al. [24], who compared the morphology of EAFS with limestone to be used as an aggregate in the production of asphalt. In Figure 2c, vitrified

surface can be observed, associated with materials exposed to high temperatures (higher than 1600 °C) inferring possible pozzolanicity and reactivity to alkali activation. In Figure 2d, the EDS test was carried out, the results of which are presented in Figure 3. The elemental composition of the EAFS corresponds to around 50.6% of oxygen, followed by calcium with a 18.0%, 7.1% for silicon and 6.2% for iron. These components are in accordance with the mineralogical composition of the XRD of EAFS (in the following section) and with other studies, like Ozturk et al. and Arribas et al. [25, 26], in which the slag is characterized by a high content of free calcium, showing as white particles in SEM, followed by silicon oxide and iron oxide.

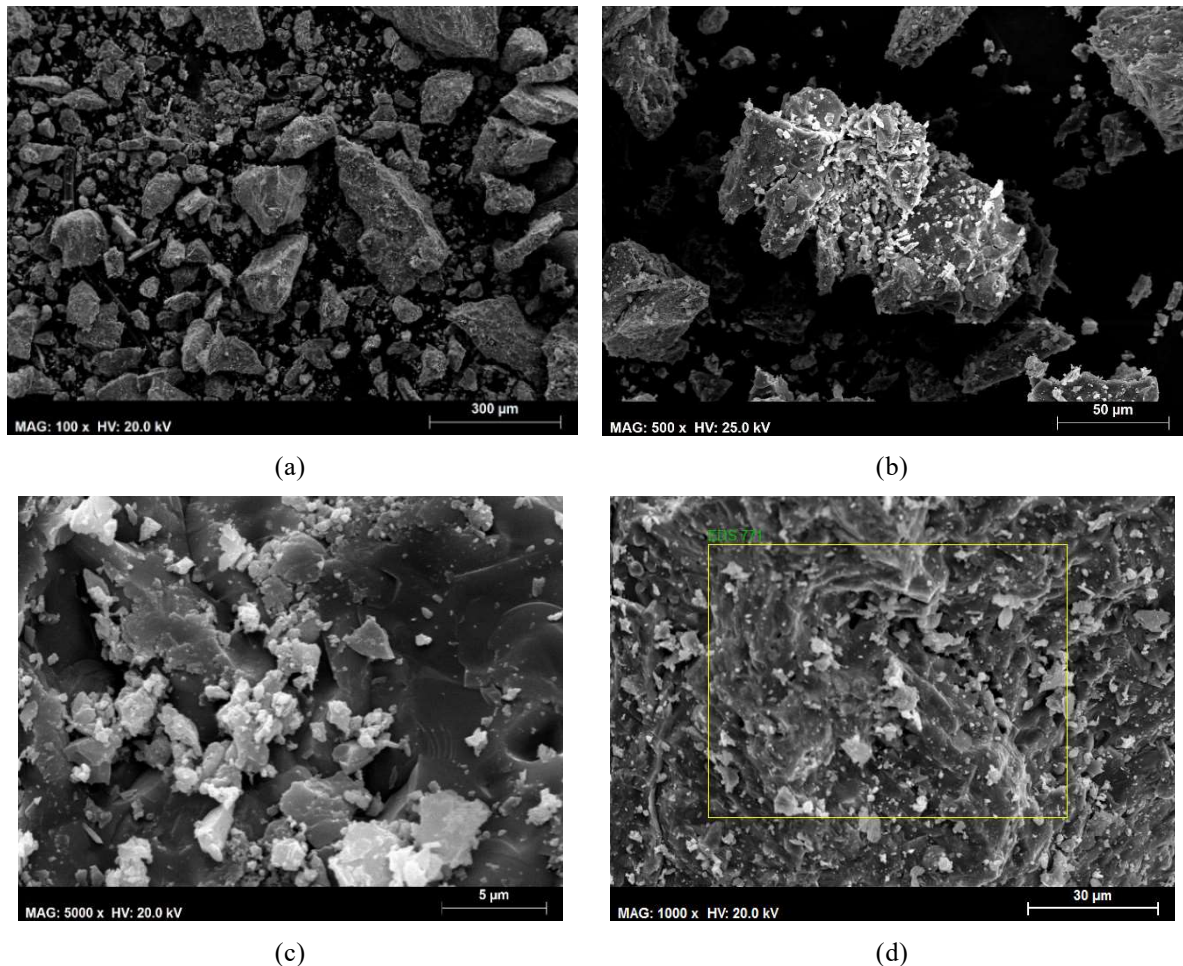


Figure 2 - SEM micrographs of EAFS

Regarding the morphology of SWTP (Figure 4), the particles are mostly of irregular size and compact. They may correspond to clays and salts, characteristic components of this type of waste.

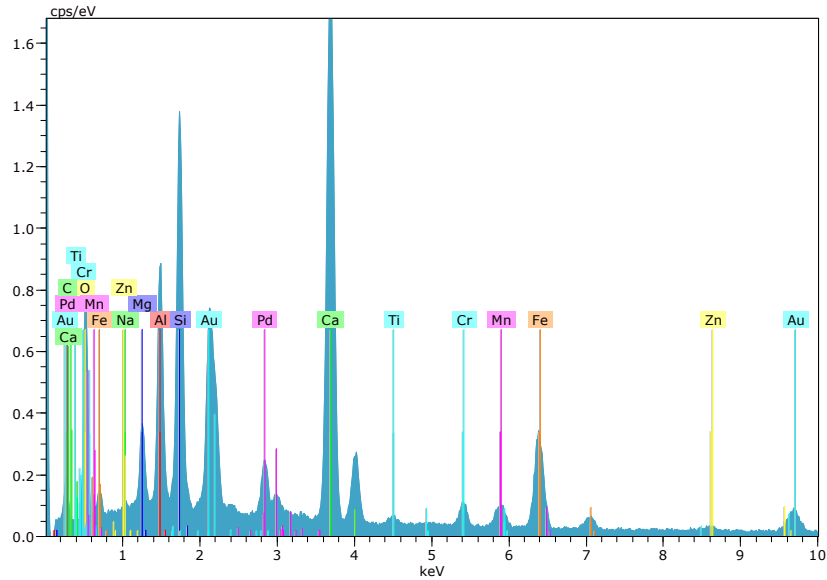
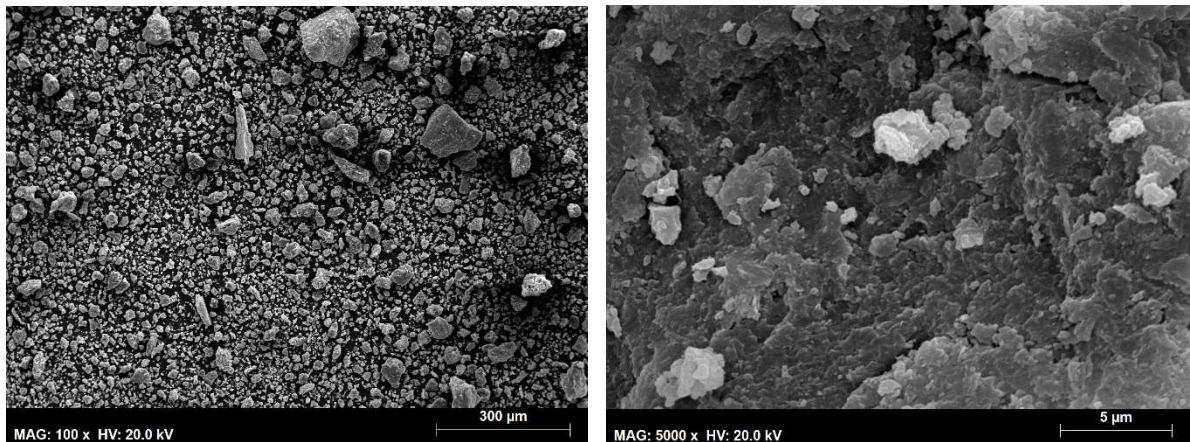


Figure 3 - EDS coupled to SEM of EAFS



(a)

(b)

Figure 4 - SEM micrographs of untreated SWTP

This result is consistent with other authors like Wang et al. [27], who compared SWTP microstructures and pulverized fly ash, the latter being spherical. In this work, Wang et al. use SWTP as a replacement for fine aggregate for the production of concrete. Another case study is that presented by Ling et al. [28], who evaluated the reuse of sludge with a rough texture as a substitute for clay in ceramic products. The microstructure of this by-product is directly related with the type of soil with which the collection water has contact. In this case, the sedimentary soil is mostly detrital limestone and clay. The EDS test was carried out, and its results are

presented in Figure 5. The elemental composition of the SWTP corresponds to around 24.4% of oxygen, followed by aluminium with 18.0%, 6.2% for calcium, 5.5% for silicon, and 2.8% for iron. These components are in accordance with other studies, as reported by Ahmad et al. [29] in its review article in which all sludges characterized present as one of the main major components aluminum oxide, Al_2O_3 (average of 20.93%).

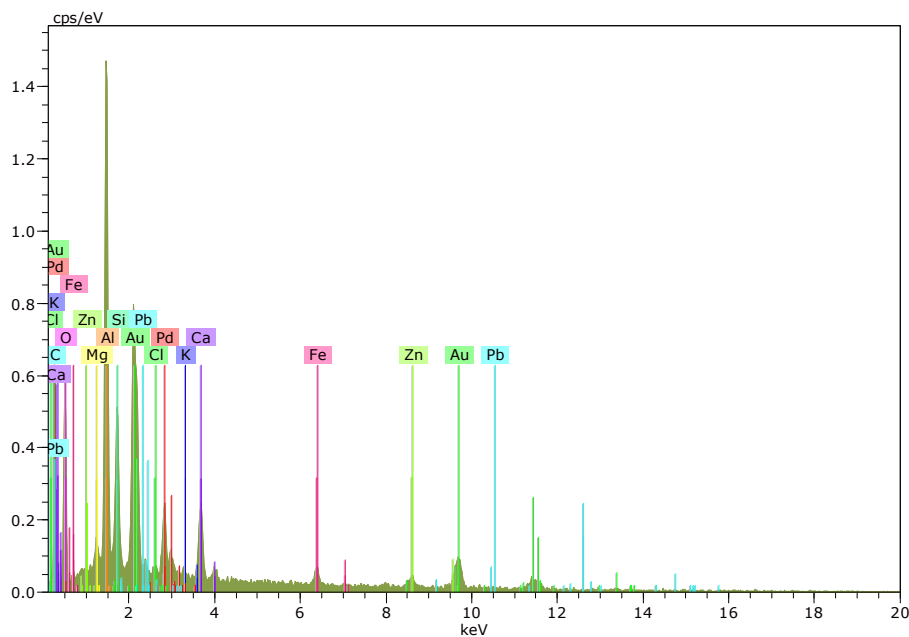


Figure 5 - EDS coupled to SEM of untreated SWTP

Figure 6, which presents the SEM of ASWTP, shows that the particles present a regular distribution in terms of size; however, they are highly porous, which results in a less dense material. Additionally, this morphology suggests a greater surface area, which could influence the absorption of water, increasing the amount required for the hydration of the particles. The elemental composition of the ASWTP corresponds to around 20.7% for oxygen, followed by aluminium with 20.0%, 13.6% for calcium, 6.4% for silicon and 1.2% for iron, which are similar values to those for the sludge without treatment. Tantawy [30] characterized sludge calcined to 600 °C and 900 °C, where he mentions that high temperatures allow dehydration of the $Al(OH)_3$, subsequent formation of Al_2O_3 and crystallization of amorphous silica.

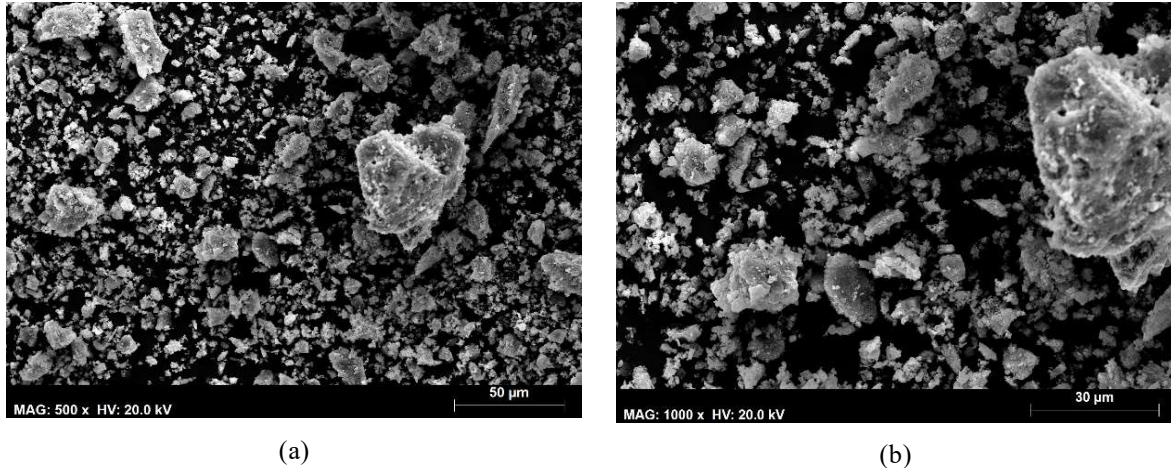


Figure 6 - SEM micrographs of ASWTP: (a) 500 amplification; (b) 1,000 amplification

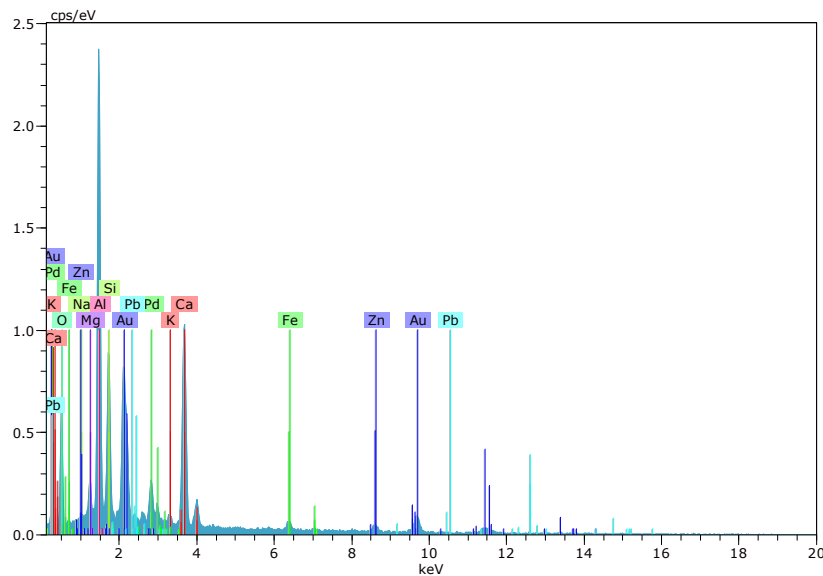


Figure 7 - EDS coupled to SEM for ASWTP treated at 700 °C

The morphology of MIBA can be seen in Figure 8, in which the prominence of particles exhibiting angular shape and with porous microstructure is easily observed. This agrees with that reported by Lynn et al. [31] and Silva et al. [32], both works corresponding to literature reviews. Like ASWTP, it is probable that a greater amount of water is needed to cover the particles' surface area for a given workability. EDS test was carried out and its results are presented in Figure 9. The elemental composition of MIBA corresponds to around 23.3% for oxygen, followed by calcium with 15.2%, 8.7% for silicon, 6.6% of aluminium and 4.1% of iron.

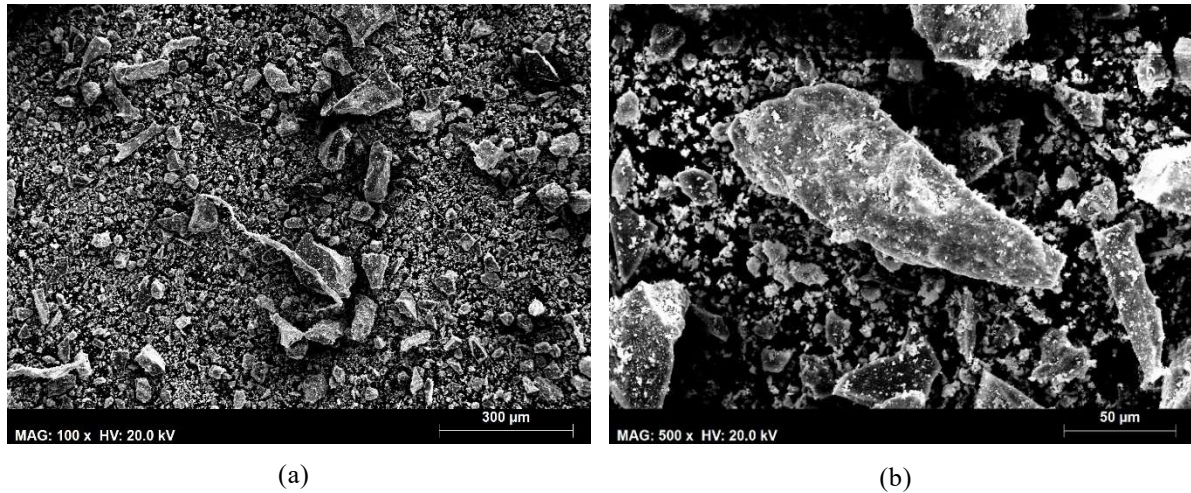


Figure 8 - SEM micrographs of MIBA

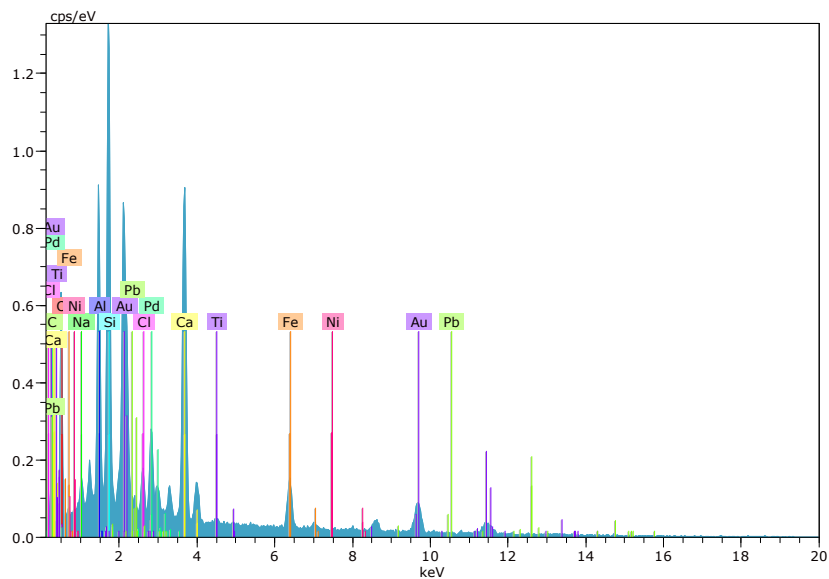


Figure 9 - EDS coupled to SEM of MIBA

3.1.2 X-ray diffraction

The XRD test was carried out in the Department of Mining Engineering of the IST, in the X-ray diffraction equipment, copper anode material, at a measuring temperature of 25 °C, with a diffractometer Type No. 0000000011019195.

Figure 10a shows the crystalline structures present in SWTP. The presence of mineral calcite

(CaCO_3) and quartz (SiO_2) is mostly observed. These phases are also present in the ASWTP (Figure 10b), which presents other phases such as andradite ($\text{Ca}_3\text{Fe}_2(\text{SiO}_4)_3$) and mayenite ($\text{Ca}_{12}\text{Al}_{14}\text{O}_{33}$). Ahmad et al. [29], in his revision article, mentions that SiO_2 was the major crystalline solid identified in numerous XRD analyses in waterworks sludge, but in this project the intensity of the peak is higher in the calcite crystal, which indicates characteristics present in the pumped water, such as high hardness that results from being in contact with calcareous means. The aluminium content in this type of waste comes mainly from the water purification process, in which aluminium salts (aluminium sulphate - $\text{Al}_2(\text{SO}_4)_3$) are usually used as a coagulant of the colloids present in the raw water. The quality of the catchment water, linked to the types of soils that come into contact with the source of uptake, can be measured based on the mineralogical phases determined in this test. The XRD of MIBA shows that the main crystalline phases were, silica (SiO_2), calcite (CaCO_3) and calcium oxide (CaO) (Figure 11). These crystalline phases were found in the samples after the incineration process of MIBA up to 1000 °C, and the silica content and CaO corroborates the results obtained in the microstructural analysis by SEM, since silicon oxide is a highly porous material, represented by thermally fractured particles[33], and calcium oxide is the product of thermal decomposition of CaCO_3 , which also generates CO_2 . This gas, once it is released, helps increase the porosity of the material.

Bayuseno et al. [33] analysed the mineralogical properties of MIBA, a by-product of the incinerator plant of Iserlohn, Germany, in which the main crystalline phases found were quartz (SiO_2), characteristic of refractories and glass fragments, corundum (Al_2O_3) and magnetite (Fe_3O_4), characteristics of high temperature combustion of metallic elements and calcite (CaCO_3), characteristic of thermal decomposition of building materials. Except for the presence of metal crystals, the results of this study, as well as those presented by Chen et al. [34], are similar to those of the MIBA studied in this report.

Finally, the X-ray diffraction of the EAFS shows that the main crystals found in this by-product are: plustite (W, FeO), gehlelite ($\text{Ca}_2\text{Al (AlSiO}_7)$), calcium silicate (Ca_2SiO_4), magnetite ($\text{Fe}^{2+} \text{Fe}^{3+} 2\text{O}_4$) and larnite, the latter also corresponds to calcium silicate (Figure 12). These characteristics make slag a potential precursor to alkaline activation, because this test confirms the

presence of the main compounds that react with the alkaline activator to produce the cementitious gel (C.A.S.H). The slag generated in Portugal has crystalline phases similar to the slags characterized by Santamaria et al. [23] and Ozturk et al. [25].

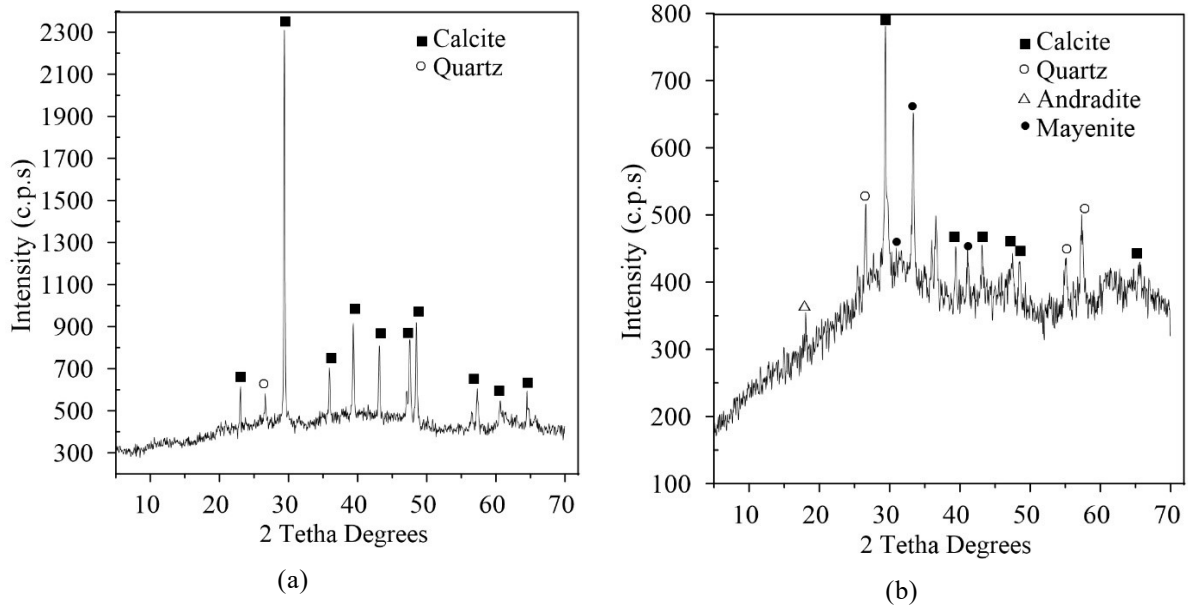


Figure 10 - XRD pattern of SWTP (a) and ASWTP (b)

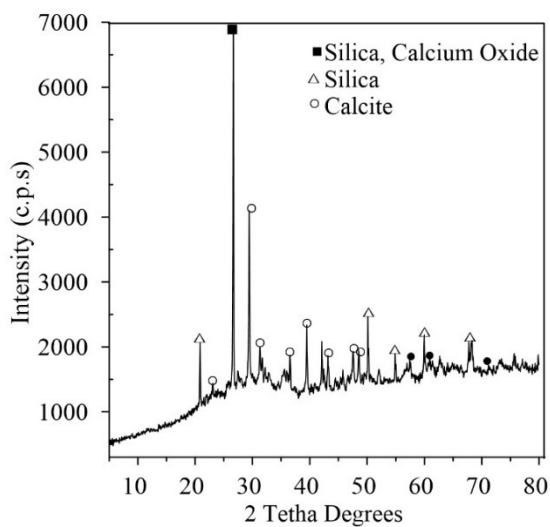


Figure 11 - XRD pattern of MIBA

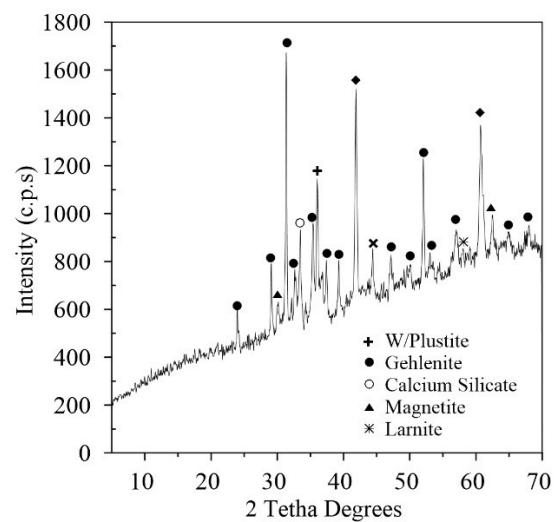


Figure 12 - XRD pattern for EAFS

3.1.3 XRF

XRF shows that MIBA contains a high content of silicon oxide (SiO_2), calcium oxide (CaO), followed by iron oxide (Fe_2O_3) and aluminium oxide (Al_2O_3). This characterization confirms the results obtained by XRD and SEM (Table 2). The sum of oxides Al_2O_3 , SiO_2 and Fe_2O_3 , according to the American standard [35] would allow the use of MIBA, classifying it as Fly ash class C (high calcium concentration), where the minimum value of the sum of the oxides (Al_2O_3 , SiO_2 and Fe_2O_3) is 50%. Lynn et al [31] showed that 66% of the MIBAs satisfy this limit. Johnson [36] compared the chemical composition of MIBA with igneous rocks, concluding that both of which are mainly made up of Si, Ca and Al.

From the characterization by XRF, it is possible to determine that this precursor corresponds to a calcium-rich system, according to the classification established by Torgal et al. [37] in the Handbook of Alkali-Activated Cements, Mortars and Concretes.

Table 2 - Chemical composition of MIBA (% by mass)

Materials	MIBA (%)
Al_2O_3	4.10
CaO	22.99
Fe_2O_3	9.21
K_2O	1.57
MgO	2.37
Na_2O	2.40
SiO_2	51.84
SO_3	2.42
Cl	0.70
Insoluble residue	-
LOI	2.40

3.1.4 pH

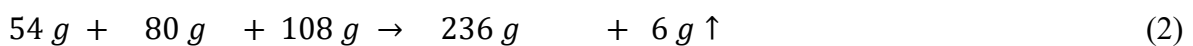
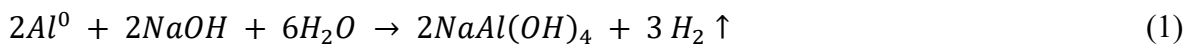
The pH test was carried out using a digital pH measurement instrument HACH brand. The procedure for pH determination in soils based on ASTM D4972 was used [38]. The by-product with

the highest hydrogen potential corresponds to EAFS, with a pH of 10.0, followed by MIBA with a pH of 9.61, ASWTP with a pH of 9.46, and finally SWTP, with a pH of 7.26. High pH values are associated with the presence of basic and/or alkaline compounds, such as calcium carbonate, present in all characterized by-products. According to Torgal et al. [37], basic pH's are required in alkaline activation reactions, since precursors will have greater hydraulic potential. Therefore, EAFS, followed by MIBA and later ASWTP, clearly present this characteristic.

3.1.5 Quantification of metallic aluminium in MIBA

The chemical reaction to produce gaseous hydrogen from metallic aluminium and NaOH corresponds to equation 1. In terms of the stoichiometric quantities (atomic and molecular weights), the quantities of each of the reactants and products generated in grams are presented in equation 2.

Equation 3 corresponds to the chemical reaction that results from the decomposition of sodium tetrahydroaluminate, ($2NaAl(OH)_4$) (the product of equation 1), in which it is observed that NaOH is regenerated and precipitates aluminum hydroxide $Al(OH)_3$.



From the stoichiometric quantities, it was determined that 0.11 g of $H_2 \uparrow$ were produced per gram of aluminium consumed (equation 4).

$$g H_2 \uparrow = 1 \text{ g } Al^0 \times \frac{6 \text{ g } H_2 \uparrow}{54 \text{ g } Al^0} = 0.11 \text{ g} \quad (4)$$

From the reaction of 0.1 g of metallic aluminium with a 2.5 M NaOH solution (excess reagent), the displaced volume of water was measured experimentally by the hydrogen gas produced, in an inverted test tube, which was connected by means of a glass tubing to a three-nozzle balloon.

The theoretical value corresponds to 143.03 ml.

Three runs were performed in order to determine an average and an error, where V_i , V_f , V_{exp} are initial volume of the inverted test tube, final volume of the inverted test tube and volume displaced by hydrogen respectively (Table 3). In the same way, the temperature at which the reaction was carried out corresponded to 43 °C (heat due to the exothermic reaction of NaOH in water). The density of hydrogen at 43 °C and 1 atm. of pressure is 0.0766 kg/m³ [39]. From this property and the mass of hydrogen produced per gram of aluminium, it was possible to determine the theoretical volume of hydrogen generated (equation 5).

$$v = \frac{m}{\rho}; \quad v_{H_2} = \frac{0.11 \text{ g}}{0.0000766 \text{ g/ml}} = 1436.03 \text{ ml} \quad (5)$$

In other words, one gram of metallic aluminum generates 1.436 liters of hydrogen.

Table 3 - Measurements made in triplicate for 0.1 g of pure metallic aluminium

H ₂ release per 0.1 g of Al ^o		
V _i (ml)	V _f (ml)	V _{exp} (ml)
10	142	132
30	156	126
28	164	136
Average		131.33
SD		5.03
Error		8%

The test was carried out again, this time with 10 g of MIBA and 800 ml of a 2.5 M NaOH solution in order to quantify the volume of hydrogen produced and subsequently the amount of metallic aluminum in grams per kg of MIBA. The results are presented in Table 4.

Using the density property (equation 6), the milligrams of hydrogen present in 63.33 ml of the gas were determined.

$$v \times \rho = m; \quad 63.33 \text{ ml} \times 0.0000766 \frac{\text{g}}{\text{ml}} = 0.00485 \text{ g} = 4.85 \text{ mg } H_2 \quad (6)$$

Table 4 - Measurements made in triplicate for 10 g of MIBA

H ₂ release per 10 g of MIBA		
Vi (ml)	Vf (ml)	Vexp (ml)
138	200	62
120	184	64
62	126	64
Average		63.33
SD		1.15

Using the stoichiometric amounts, the amount of metallic aluminium that produces this amount of hydrogen is determined (equation 7).

$$g Al^{\circ} = 0.00485 g H_2 \uparrow \times \frac{54 g Al^{\circ}}{6 g H_2 \uparrow} = 0.04365 g Al^{\circ} \quad (7)$$

In other words, 10 grams of MIBA contain 43.65 mg of metallic aluminium. Thus, it can be concluded that there is 4.36 g of Al per kg of MIBA and this aluminium, in contact with an excess NaOH solution, produces 6.3 L of H₂↑ per kg of MIBA. Figure 13 presents the relationship of hydrogen released by MIBA over time in minutes.

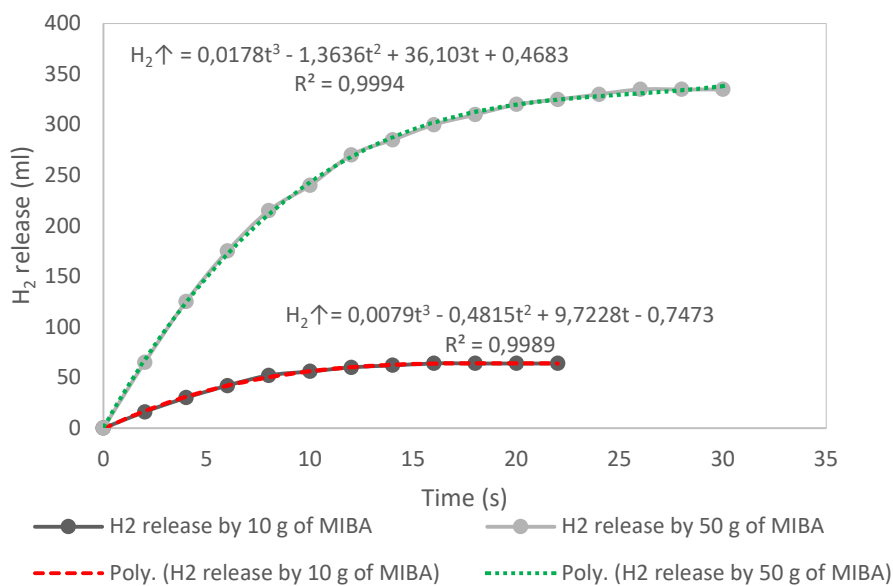
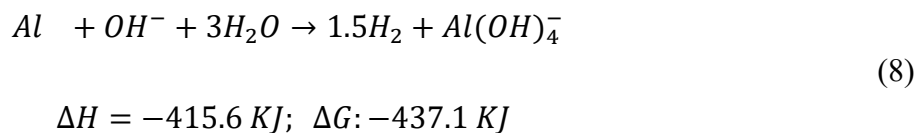


Figure 13 - Hydrogen production over time of MIBA samples

The figure allows inferring that the relationship between the time of release of the gas and the volume of hydrogen released for different amounts of MIBA does not follow the same mathematical model, since despite the trend lines (H_2 released by 10 g of MIBA and H_2 released by 50g of MIBA) being polynomials of third order, the coefficients are different. Therefore, the use of chemical kinetics is determinant in order to evaluate the speed of the reaction, making the model applicable to any amount of MIBA.

In terms of the thermodynamics of the reaction, reaction (1) proceeds in the following way (equation 8):



The negative value of the enthalpy (-415.6 kJ) indicates that the reaction is exothermic, which indicates that the high temperatures favour the speed of the product's formation. Gibbs' free energy, which also has a negative value ($\Delta G: -437.1 \text{ kJ}$), indicates that the reaction is spontaneous, so that hydrogenation does not require energy supply to occur.

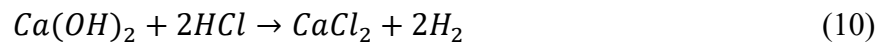
The heat produced in this reaction is as follows: 15.37 kJ are generated for each gram of metallic Al (aluminium atomic mass: 27 UMA). If in this MIBA sample there are 4.36 g of Al per kg of MIBA, in 450 grams of MIBA (quantity used for mortars) there are 1.952 g of Al, which produce 2.83 L of hydrogen. For these quantities, 30.15 kJ are produced. The temperature of the reaction was $43 \text{ }^\circ\text{C}$. The heat released by the reaction was absorbed by the water, which was used as a factor to accelerate the reaction rate.

Aubert et al. [11] quantified the metallic aluminium present in a sample of MIBA from an incineration plant in France, obtaining values of 1.99 g Al/kg of MIBA. Likewise, Tang [10] obtained values of 6.99 g of Al/kg de MIBA and 3.72 g of Al/kg de MIBA from the Dutch incinerator plants in Wijster and Moerdijk, respectively. These results show that the values obtained in the Lisbon incineration plant are within those defined for these three countries. None of these studies presents the month of the year in which the samples were obtained, in

order to observe a consumption trend related to the amount of aluminium present in the waste.

3.1.6 Pozzolanic activity index

The modified Chappelle test determined by titration with 0.1 M HCl, the content of Ca (OH)₂ not consumed (free content) by the reactive phases present in MIBA during 16 h of reaction at 90 ± 5 °C of 2 g CaO grade laboratory and one gram of the by-product diluted in distilled water. The reactions presented in the titration are the following (equations 9 and 10):



Thus, through equation 11, it is possible to calculate the mg Ca (OH)₂ / g of by-product [40]:

$$\frac{mg \text{ Ca(OH)}_2}{g \text{ by-product}} = \frac{28 \times (v_3 - v_2) \times F_c}{m_2} \times 1.32 \quad (11)$$

Where m_2 is the mass of the pozzolanic material expressed in grams, v_2 the volume of HCl consumed by the sample; v_3 the volume of HCl consumed by the blank; F_c , correction factor for a 0.1 M solution and 1.32 the molecular relationship Ca (OH)₂ / CaO.

Through the Chappelle test, a value of 445 mg of Ca(OH)₂ per g of MIBA was obtained, which is higher than the minimum limit, 436 mg Ca(OH)₂/g of addition established by Raverdy et al. [41, 42], for the classification of a mineral addition as a pozzolanic material, concluding that both by-products can be considered as pozzolanic, which is confirmed by Tyrer [13], in his work on the use of MIBA in concrete, where he mentions that MIBA shows pozzolanic activity when it is finely pulverized, and Filipponi et al. [43] who conclude that MIBA has low pozzolanic activity.

3.2 Fresh state properties

3.2.1 Density

The fresh density for all control mixes reveals that all values vary between 1.6 g/ml and 1.85

mg/ml for MIBA and 1.90 g/ml and 1.95 g/ml for EAFS (Figure 14).

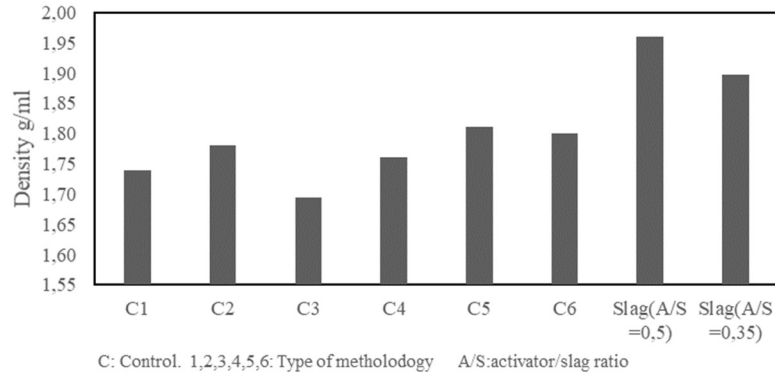


Figure 14 - Density in the fresh state

MIBA mortars in the fresh state have lower density values than ordinary Portland cement mortars; therefore, it can be inferred that MIBA has a lower density than Ordinary Portland Cement (3.15 g/ml). This may be explained by the release of hydrogen gas from the reaction of aluminum with sodium hydroxide, generating bubbles in a plastic state; at the same time, MIBA has a low density, since the process of generation of the by-product involves high temperatures, which make its microstructure porous due to the release of gases associated mainly with organic matter [44]. The density of slag compared to that of MIBA control mixes is slightly higher, which means that in the fresh and hardened states the mixes are more compact. The results, such as those reported by Chen et al. [34], confirm the tendency of this property in the hardened state, since in the work mentioned above the dry density of the geopolymer produced with MIBA ranges between 0.676 g/ml and 0.10 g/ml. These values depend on the MIBA/alkaline activator ratio: the higher the ratio, the more the density decreases in the hardened state. On the other hand, Jinyoung et al. [45] determined the density in the fresh state for cement pastes with MIBA replacement as mineral addition. The reported values range between 1.718 g/ml and 1.878 g/ml, corresponding to a paste with 30% replacement and the control paste respectively, confirming the decrease in density caused by MIBA.

Figure 15 shows the density in the fresh state of M1, M2 and M3, making use of different water reducing admixtures. In every case, it is observed that the higher density in the fresh state

corresponds to the family P and L. behaviour contrary to the superplasticizer N and M. The P and L families are classed as superplasticizers. According to the literature, P generates the greatest fluidity in the mixes, and is classified as a high-ranking water reducing agent [46]. L comes mainly from organic sources of cellulose [47], which classification depends on the type of cellulose they come from and generally leads to high fluidity, contrary to N and M; which have similar behaviours. Topçu and Ateşin [48], in their research work on mortars, make a comparison between L and N, finding results similar to those reported in the present work, since the mixes made with L report densities in the fresh state higher than those made with N.

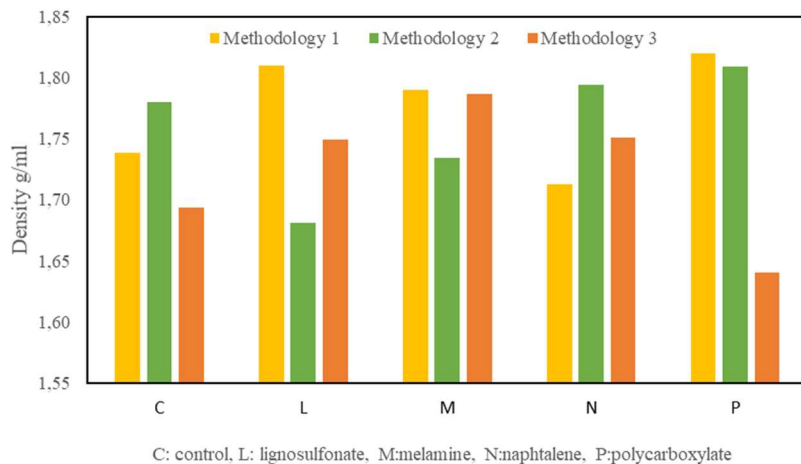


Figure 15 - Density in the fresh state of M1, M2 and M3

3.2.3 Workability

Figure 16 shows the values obtained for the workability of all mortars. The mixes with the highest workability are those made with lignosulfonate and polycarboxylate, followed by those made with naphthalene and finally melamin. All the control mixes are classified as dry mortar, which indicates the need of the use of a water reducing agent to reach a classification of plastic state according to the standard [22]: 140 mm < spread < 200 mm).

In the case of slags, an alkaline activator/slag ratio of 0.5 causes a highly fluid mix, so it was possible to measure the spread diameter.

This result may be related to the MIBA's microstructure, whose particles, having an angular

and porous shape, may require a higher water content to obtain a plastic mortar without the aid of the water reducing admixtures, as explained by Tyrer [13].

The tendency with respect to the use of water reducing agents is similar to that obtained for density, considering that families M and N have similar behaviours, and P and L have better performance. Topçu and Ateşin [48] evaluated this property, finding that N mortars had the best performance.

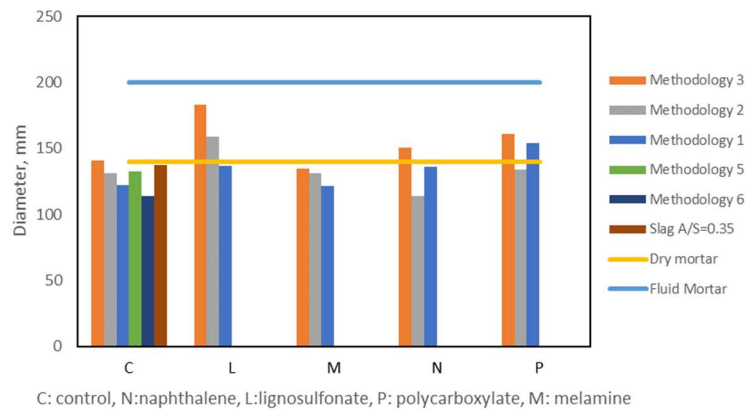


Figure 16 - Workability of the mortars

3.3 Hardened state performance

3.3.1 Compressive strength

Figure 17 and Figure 18 show the results of all mortars and proposed methodologies, including EAFS. For the mixes with MIBA, the best results in the compressive strength were obtained in mortars C5 and C and the worst ones in mortars L2 and P3, at both 7 and 28 days. According to Garcia et al [5], for both precursors the main reaction product corresponds to C.A.S.H gel, $((Na,K)_2O-CaO-Al_2O_3-SiO_2-H_2O)$.

This behaviour is directly related with the main chemical reaction that occurs (equation 1), which can be accelerated by the following factors: pressure, temperature, catalysts and concentration of reagents.

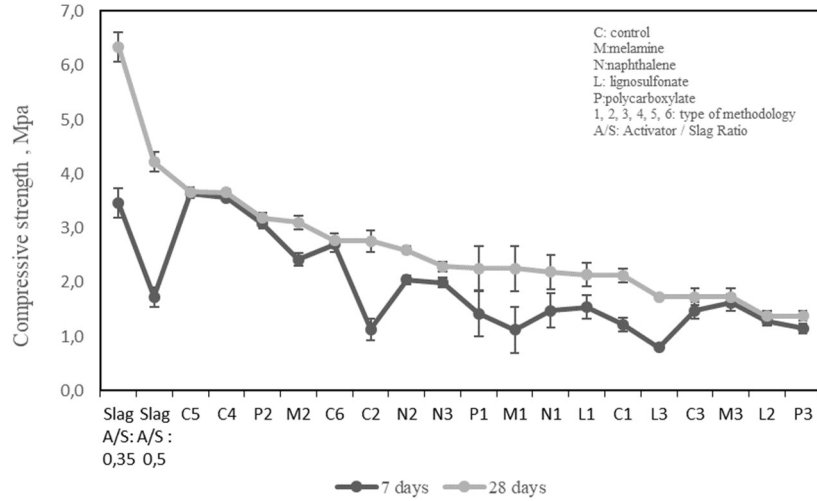


Figure 17 - Compressive strength of all mortars

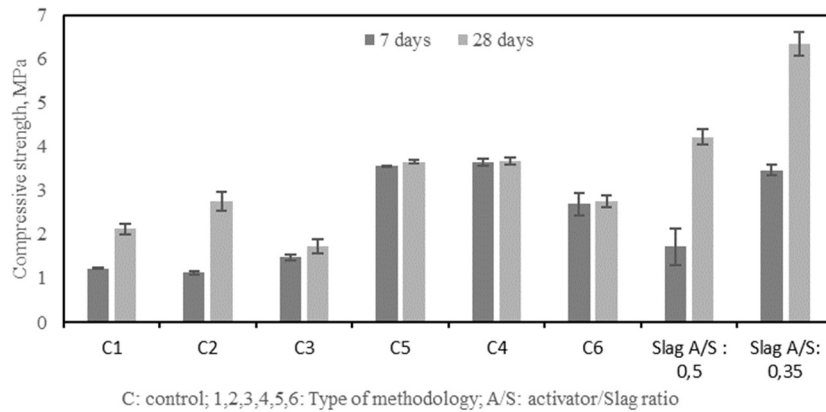


Figure 18 - Compressive strength of the control mixes

The heat of reaction (Q) for methodologies 4 and 5 is 28.14 kJ and 23.45 kJ respectively. An example of calculation is presented in equation 12, where C : heat capacity of water in (kJ/kg.K); t_1 : initial temperature of the solution preparation water; t_2 : final solution temperature after NaOH is added and m : water weight.

$$c = 4.169 \frac{\text{kJ}}{\text{kg} * \text{K}} \quad t_1: 18^\circ\text{C} \quad t_2: 43^\circ\text{C} \quad m: 0.225 \text{ kg} \quad (12)$$

$$Q = mc\Delta t = 23.45 \text{ kJ}$$

At constant pressure, $Q = 23.45 \text{ kJ}$ corresponds to the reaction enthalpy.

Since the reaction is exothermic (equation 8), it is possible to take advantage of the heat generated by the dissolution of NaOH in water to accelerate the reaction of H₂ production.

The heat absorbed by the water when it reacts with NaOH is used to accelerate the reaction rate of the alkaline activator with the metallic aluminum present in MIBA. The high temperature expands the gases; therefore, when the mix is allowed to rest in the plastic state for an additional time, all hydrogen is released and the temperature decreases. 24 hours later, the gases trapped in the mixture are released by means of mechanical stirring.

This result is consistent with that of Poon et al. [49], who state that some metallic Al removal treatments take some time, from a few days to weeks.

Low compressive strength after alkaline activation of MIBA, such as that presented in this report (maximum of 3.67 MPa at 28 days), is consistent with the results of various authors, such as Chen et al. [34], who developed a geopolymer with a maximum compressive strength of less than 3 MPa, or Silva et al. [32], who in their review paper found that the maximum compressive strength obtained after alkaline activation of MIBA does not exceed 3 MPa.

Another field of research, still unexplored in terms of alkaline-activated materials with MIBA as precursor, is the use of catalysts, which are inhibitory substances, such as the following plants, that eliminate H₂ in the chemical reaction of metallic aluminum and aqueous NaOH: *Gume Arabic* [50] or *Impomea involcrata* [51]. However, the reactivity of these inhibitors with natural aggregates or with other amorphous phases has not been proven.

It is necessary to check through analytical techniques whether the aluminum hydroxide of equation 3 is in a crystalline or amorphous state, in order to evaluate its reactivity, since there are investigations where adding amorphous aluminum in the form of aluminum hydroxide improves the mechanical properties of the alkali activated material, in which the strength increased [52].

On the other hand, EAFS with a high Ca content, such as MIBA, do not contain metallic aluminum. For this reason, the compressive strength in EAFS mortars is greater than in MIBA mortars. Figure 19, Figure 20, and Figure 21 present the compressive strength at 7 and 28 days obtained for methodologies 1, 2 and 3 with four different water reducing agents. In all the graphs, the mortars with lignosulfonate have the lowest strength at 28 days; in the case of melanin, naphthalene and

polycarboxylate mortars, the behaviour does not present a trend related to the mixing methodology used. This indicates that this variable does not have a high influence on compressive strength in alkali activated materials. Gamal et al. [53] concluded that naphthalene slightly improves the mechanical properties of ordinary Portland cement pastes.

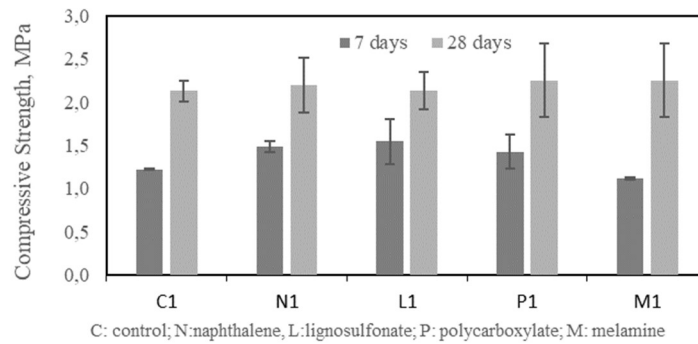


Figure 19 - Compressive strength of the mortars for methodology 1

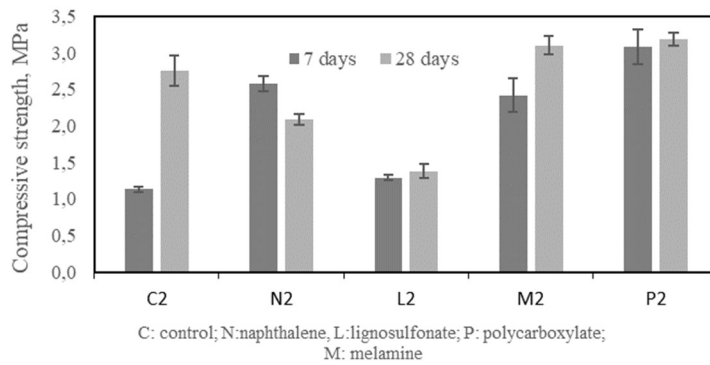


Figure 20 - Compressive strength of the mortars for methodology 2

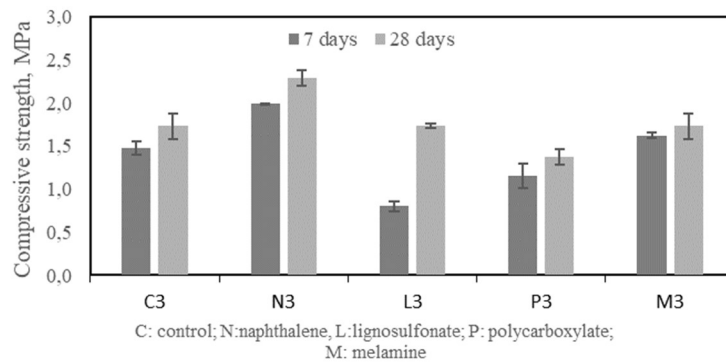


Figure 21 - Compressive strength of the mortars for methodology 3

3.3.2 Flexural strength

The flexural strength for all methodologies proposed at 7 and 28 days was determined. Figure 22 shows that the control mixes of methodology 4 and 5 have the highest values of flexural strength at 28 days: 0.727 MPa and 0.797 MPa respectively. The mortar made with slag had the highest flexural strength, 0.798 MPa.

Figure 23, Figure 24, and Figure 25 present the flexural strengths at 7 and 28 days for methodologies 1, 2 and 3 and four admixtures. In all figures, the mortars with lignosulfonate have the lowest flexural strengths at 28 days (L2 and L3 broke at demoulding, so the tests could not be performed). In melanin, naphthalene and polycarboxylate mortars, the behaviour does not present a trend related to the mixing methodology used. This indicates that this variable does not have a high influence on compressive strength, but it has a great influence on workability.

Flexural strength behaviour can be explained similarly to compressive strength.

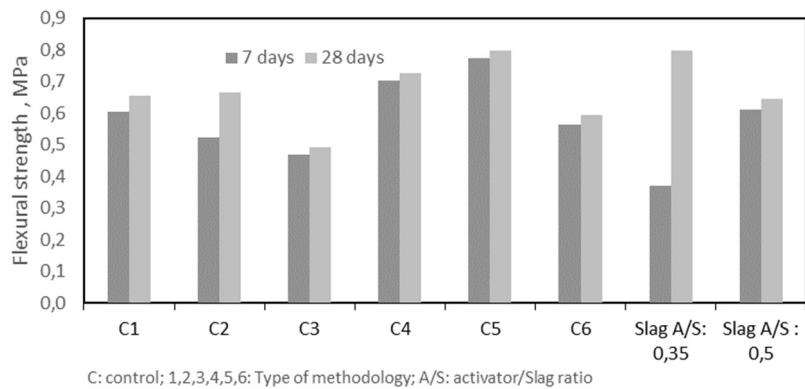


Figure 22 - Flexural strength of the control mortars

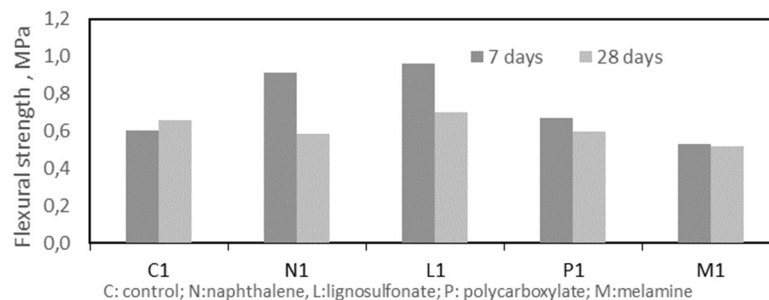


Figure 23 - Flexural strength of the mortars for methodology 1

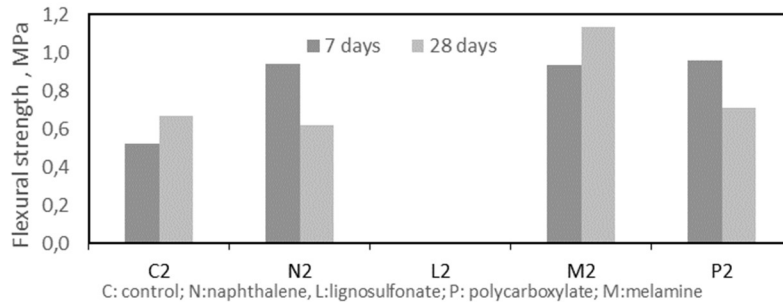


Figure 24 - Flexural strength of the mortars for methodology 2.

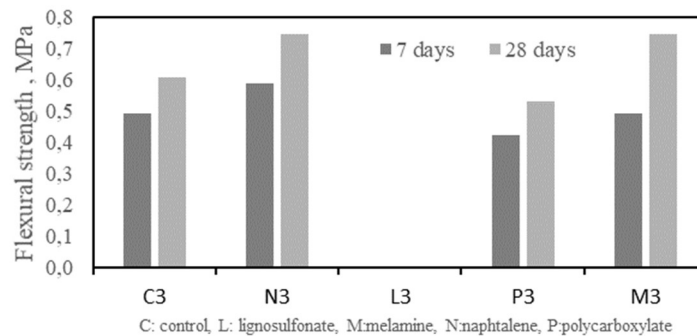


Figure 25 - Flexural strength of the mortars for methodology 3

4 CONCLUSIONS

The by-products characterized present properties that make them potential precursors of alkaline activation, such as basic pH, and presence of crystalline compounds with constituents of calcium, silicon and aluminum.

All precursors analyzed, once activated, will lead to the formation of the C.A.S.H gel, because in all the calcium content is much higher.

It is necessary to use a superplasticizer to reach the plastic category for fresh mortars, which can be either naphthalene or polycarboxylate.

As for MIBA mortars, the best methodology to produce an alkaline activated material and in which hydrogen release is controlled with the lowest energy expenditure is number 5.

The electric furnace slag with low concentrations of NaOH yields better compressive strength results (6.35 MPa at 28 days of curing age), with a low activator/slag ratio of 0.35. Therefore,

it is recommended to evaluate the use of this by-product to improve the mechanical properties of the material.

It is recommended to quantify the amorphous contents in the precursors, since these are the phases that react with the activator producing the geopolymer.

REFERENCES

1. Provis, J.L., *Alkali-activated materials*. Cement and Concrete Research, 2018. **114**: p. 40-48.
2. Torres-Carrasco, M. and F. Puertas, *Alkaline activation of aluminosilicates as an alternative to portland cement: a review*. Revista Romana de Materiale-Romanian Journal of Materials, 2017. **47**(1): pp. 3-15.
3. Pacheco-Torgal, F., J. Castro-Gomes, and S. Jalali, *Alkali-activated binders: A review - Part 1. Historical background, terminology, reaction mechanisms and hydration products*. Construction and Building Materials, 2008. **22**(7): pp. 1305-1314.
4. Pacheco-Torgal, F., J. Castro-Gomes, and S. Jalali, *Alkali-activated binders: A review. Part 2. About materials and binders manufacture*. Construction and Building Materials, 2008. **22**(7): p. 1315-1322.
5. Garcia-Lodeiro, I., A. Palomo, and A. Fernández-Jiménez, *An overview of the chemistry of alkali-activated cement-based binders*, in *Handbook of alkali-activated cements, mortars and concretes*. 2015, Elsevier. pp. 19-47.
6. Fernández-Jiménez, A., et al., *Quantitative determination of phases in the alkaline activation of fly ash. Part II: Degree of reaction*. Fuel, 2006. **85**(14): pp. 1960-1969.
7. Chen-Tan, N.W., et al., *Determining the reactivity of a fly ash for production of geopolymer*. Journal of the American Ceramic Society, 2009. **92**(4): pp. 881-887.
8. Williams, R.P. and A. van Riessen, *Determination of the reactive component of fly ashes for geopolymer production using XRF and XRD*. Fuel, 2010. **89**(12): pp. 3683-3692.
9. Khale, D. and R. Chaudhary, *Mechanism of geopolymerization and factors influencing its development: a review*. Journal of Materials Science, 2007. **42**(3): pp. 729-746.
10. Tang, P., *Municipal solid waste incineration (MSWI) bottom ash - from waste to value. characterization, treatments and application*. Eindhoven: Technische Universiteit Eindhoven 2017
11. Aubert, J.E., B. Husson, and A. Vaquier, *Metallic aluminum in MSWI fly ash: quantification and influence on the properties of cement-based products*. Waste Management, 2004. **24**(6): pp. 589-596.

12. Xuan, D., P. Tang, and C.S. Poon, *Limitations and quality upgrading techniques for utilization of MSW incineration bottom ash in engineering applications - A review*. Construction and Building Materials, 2018. **190**: pp. 1091-1102.
13. Tyrer, M., *Municipal solid waste incinerator (MSWI) concrete*, in *Eco-Efficient Concrete*. 2013, pp. 273-310.
14. Qiao, X., et al., *Novel cementitious materials produced from incinerator bottom ash*. Resources, conservation and recycling, 2008. **52**(3): pp. 496-510.
15. Rübner, K., F. Haamkens, and O. Linde, *Use of municipal solid waste incinerator bottom ash as aggregate in concrete*. Quarterly Journal of Engineering Geology and Hydrogeology, 2008. **41**(4): pp. 459-464.
16. Garcia-Lodeiro, I., et al., *Manufacture of hybrid cements with fly ash and bottom ash from a municipal solid waste incinerator*. Construction and Building Materials, 2016. **105**: pp. 218-226.
17. Garcia-Lodeiro, I., A. Palomo, and A. Fernández-Jiménez, *Crucial insights on the mix design of alkali-activated cement-based binders*, in *Handbook of alkali-activated cements, mortars and concretes*. 2015, pp. 49-73.
18. BSI, *BS EN 12620: Aggregates for concrete*. 2002, BSI London, UK.
19. Dudoladov, A., et al., *Generation of hydrogen by aluminium oxidation in aqueous solutions at low temperatures*. international journal of hydrogen energy, 2016. **41**(4): pp. 2230-2237.
20. Liu, Y., et al., *Alkali-treated incineration bottom ash as supplementary cementitious materials*. Construction and Building Materials, 2018. **179**: pp. 371-378.
21. EN, N., *196-1 (2006)-Métodos de ensaio de cimentos*. Parte 1.
22. UNE, E., *1015-3. Métodos de ensayo de los morteros para albañilería. Parte 3: Determinación de la consistencia del mortero fresco (por la mesa de sacudidas)*. 1998, AENOR Madrid.
23. Santamaria, A., et al., *Dimensional stability of electric arc furnace slag in civil engineering applications*. Journal of Cleaner Production, 2018. **205**: pp. 599-609.
24. Alinezhad, M. and A. Sahaf, *Investigation of the Fatigue characteristics of Warm Stone Matrix Asphalt (WSMA) Containing Electric Arc Furnace (EAF) Steel Slag as Coarse Aggregate and Sasobit as Warm Mix Additive*. Case Studies in Construction Materials, 2019: pp. e00265.
25. Ozturk, M., et al., *Alkali activation of electric arc furnace slag: Mechanical properties and micro analyzes*. Journal of Building Engineering, 2019. **21**: pp. 97-105.
26. Arribas, I., et al., *Electric arc furnace slag and its use in hydraulic concrete*. Construction and Building Materials, 2015. **90**: pp. 68-79.

27. Wang, L., et al., *A novel type of controlled low strength material derived from alum sludge and green materials*. Construction and Building Materials, 2018. **165**: pp. 792-800.
28. Ling, Y.P., et al., *Evaluation and reutilization of water sludge from fresh water processing plant as a green clay substituent*. Applied Clay Science, 2017. **143**: pp. 300-306.
29. Ahmad, T., K. Ahmad, and M. Alam, *Sustainable management of water treatment sludge through 3 'R' concept*. Journal of Cleaner Production, 2016. **124**: pp. 1-13.
30. Tantawy, M.A., *Characterization and pozzolanic properties of calcined alum sludge*. Materials Research Bulletin, 2015. **61**: pp. 415-421.
31. Lynn, C.J., R.K. Dhir, and G.S. Ghataora, *Municipal incinerated bottom ash use as a cement component in concrete*. Magazine of Concrete Research, 2017. **69**(10): pp. 512-525.
32. Silva, R.V., et al., *Use of municipal solid waste incineration bottom ashes in alkali activated materials, ceramics and granular applications: A review*. Waste Management, 2017. **68**: pp. 207-220.
33. Bayuseno, A.P. and W.W. Schmahl, *Understanding the chemical and mineralogical properties of the inorganic portion of MSWI bottom ash*. Waste Management, 2010. **30**(8-9): pp. 1509-1520.
34. Chen, Z., et al., *Incinerator bottom ash (IBA) aerated geopolymer*. Construction and Building Materials, 2016. **112**: pp. 1025-1031.
35. Materials, A.S.o.T., *Standard specification for coal fly ash and raw or calcined natural pozzolan for use in concrete*. 2019.
36. Johnson, C.A., S. Brandenberger, and P. Baccini, *Acid neutralizing capacity of municipal waste incinerator bottom ash*. Environmental science & technology, 1995. **29**(1): pp. 142-147.
37. Pacheco-Torgal, F., Labrincha, J., Leonelli, C., Palomo, A., & Chindaprasit, P. (Eds) *Handbook of alkali-activated cements, mortars and concretes*. Woodhead Publishing. 2014.
38. Materials, A.S.o.T., *Standard Test Methods for pH of Soils*. 2019. 6 p.
39. *Engineering ToolBox. Hydrogen - Density and Specific Weight*. 2018: https://www.engineeringtoolbox.com/hydrogen-H2-density-specific-weight-temperature-pressure-d_2044.html
40. Técnicas, A.-A.B.d.N., *NBR 15895. Materiais pozolânicos - Determinação do teor de hidróxido de cálcio fixado - Método Chapelle modificado*. 2010. 6 p.
41. Raverdy, M., et al., *Appréciation de l'activité pouzzolanique de constituents secondaires*. Proceedings of 7^{ème} congrés international de la chimie des ciments, Paris, France, 1980: pp. 6-41.

42. Hoppe Filho, J., *Atividade pozolânica de adições minerais para cimento Portland (Parte I): Índice de atividade pozolânica (IAP) com cal, difração de raios-X (DRX), termogravimetria (TG/DTG) e Chapelle modificado*. Revista Matéria, 2017. **22**(3).
43. Filipponi, P., et al., *Physical and mechanical properties of cement-based products containing incineration bottom ash*. Waste Management, 2003. **23**(2): pp. 145-156.
44. Tang, P., et al. *The application of treated bottom ash in mortar as cement replacement*. in *EurAsia Waste Manag Symp, Istanbul*. 2014.
45. Kim, J., et al., *Investigation on the side effects of municipal solid waste incineration ashes when used as mineral addition in cement-based material*. Road Materials and Pavement Design, 2016. **17**(2): pp. 345-364.
46. Lange, A., T. Hirata, and J. Plank, *Influence of the HLB value of polycarboxylate superplasticizers on the flow behavior of mortar and concrete*. Cement and Concrete Research, 2014. **60**: pp. 45-50.
47. Mbugua, R., R. Salim, and J. Ndambuki, *Effect of Gum Arabic Karroo as a water-reducing admixture in cement mortar*. Case Studies in Construction Materials, 2016. **5**: pp. 100-111.
48. Topçu, İ.B. and Ö. Ateşin, *Effect of high dosage lignosulphonate and naphthalene sulphonate based plasticizer usage on micro concrete properties*. Construction and Building Materials, 2016. **120**: p. 189-197.
49. Xuan, D. and C.S. Poon, *Removal of metallic Al and Al/Zn alloys in MSWI bottom ash by alkaline treatment*. Journal of Hazardous Materials, 2018. **344**: p. 73-80.
50. Umoren, S.A., et al., *Gum arabic as a potential corrosion inhibitor for aluminium in alkaline medium and its adsorption characteristics*. Anti-Corrosion Methods and Materials, 2006. **53**(5): pp. 277-282.
51. Obot, I. and N. Obi-Egbedi, *Ipomoea involcrata as an ecofriendly inhibitor for aluminium in alkaline medium*. Portugaliae Electrochimica Acta, 2009. **27**(4): pp. 517-524.
52. Salami, B.A., et al., *Impact of Al(OH)(3) addition to POFA on the compressive strength of POFA alkali-activated mortar*. Construction and Building Materials, 2018. **190**: pp. 65-82.
53. El-Gamal, S.M.A., F.M. Al-Nowaiser, and A.O. Al-Baity, *Effect of superplasticizers on the hydration kinetic and mechanical properties of Portland cement pastes*. Journal of Advanced Research, 2012. **3**(2): pp. 119-124.

Lisboa, 31st July, 2019

Authors

Yoleimy Ávila Pereira

PhD Candidate

Rui Vasco Silva

PhD Researcher

Jorge de Brito

Full Professor